Single atomic layer allotrope of bismuth with rectangular symmetry

P. J. Kowalczyk*
Department of Solid State Physics, Faculty of Physics and Applied Informatics, University of Lodz, 90-236 Lodz, Pomorska 149/153, Poland

O. Mahapatra, M. Le Ster, and S. A. Brown†
The MacDiarmid Institute for Advanced Materials and Nanotechnology, Department of Physics and Astronomy, University of Canterbury, Private Bag 4800, Christchurch 8140, New Zealand

G. Bian
Department of Physics and Astronomy, University of Missouri, Columbia, Missouri 65201, USA

X. Wang
College of Science, Nanjing University of Science and Technology, Nanjing 210094, China

T.-C. Chiang
Department of Physics, University of Illinois at Urbana-Champaign, 1110 West Green Street, Urbana, Illinois 61801-3080, USA
(Received 7 March 2017; revised manuscript received 19 June 2017; published 27 November 2017)

We report the observation of a new allotrope of two-dimensional bismuth. Our scanning tunneling microscopy experiments show that the structure is clearly different than the previously synthesized allotropes β- and α-bismuthene. It has a rectangular symmetry similar to that of α-bismuthene, but is composed of a puckered single monolayer of Bi atoms (α-bismuthene is intrisincally a paired layer material similar to black phosphorous). Atomic resolution images and an observed moiré pattern show that the new allotrope has a significantly contracted surface unit cell. The electronic structure is dominated by high density of states at the Fermi level as measured using scanning tunneling spectroscopy (STS) and confirmed by calculations based on density functional theory (DFT) which reveal Dirac cones at three different points in the Brillouin zone.

DOI: 10.1103/PhysRevB.96.205434

I. INTRODUCTION

The last few years have seen an intensification of the search for new two-dimensional (2D) systems, driven by discoveries of a multitude of new materials and many new physics phenomena. The starting point for this search was the exfoliation of graphene [1] which is characterized by extraordinary mechanical, thermal, and electrical properties [2–4]. More recently silicene [3–5] and germanene [3,4,6]—the silicon and germanium analogs of graphene—have been reported, as well as the germanium analog of graphane [3,4,7]. Exfoliation of many other 2D materials was also possible [3,8], including MoS_2 [9–11], WS_2 [10,11], and other transition-metal dichalcogenides [11] which are of course all compounds, in contrast to the elemental 2D materials graphene, silicene, and germanene. The other group of layered, elemental 2D materials that has been synthesized is located in the 15th group of the periodic table and includes phosphorene [3,4,12,13], black arsenic [14], β-bismuthene (β-Bi) [4,15,16] [see Fig. 1(a)], and α-bismuthene (α-Bi) [4,16–19] [see Fig. 1(b)]. In fact many other group 15 2D structures have also been proposed, including the δ, ϵ, ζ, η, θ, and ι forms of phosphorene, arsenene, antimonene, and bismuthene [16,20].

β-Bi is a hexagonal (111) structure (A7 crystallographic structure) that grows as a single monolayer [the confusing terminology "bilayer" is sometimes used to indicate that the monolayer actually comprises atoms in two distinct sites, at different heights, as shown in Fig. 1(a)]. In contrast, phosphorene and α-Bi have the black phosphorus like (BP-like) A17 structure [Fig. 1(b)]. These crystallize in the (110) orientation, with a rectangular unit cell and are *intrinsically paired* layer structures comprising *two* atomic layers that are connected by strong interlayer bonds. Both Bi(111) and Bi(110) structures are of high importance because their edges may support topologically protected edge states [21,22].

The structure shown in Fig. 1(b) makes it clear that a single monolayer of the A17 structure is not possible because the second layer is *required* to bind it together: the A17 structure can *only* exist in paired layer form. Nevertheless, in this article we provide evidence for a 2D allotrope of monolayer bismuth (MBi) with rectangular symmetry similar to that of the Bi(110) structure shown in Fig. 1(b), but with a substantially contracted surface unit cell [see Fig. 1(c)]. The MBi is physisorbed on top of α-Bi [18,19]. Our experimental STM/STS results are supported by DFT calculations which identify the minimum energy structure and show that the contracted Bi(110) unit cell is achieved through strong puckering, i.e., out-of-plane distortion of the rectangular unit cell.

II. METHODS

Commercially available HOPG (SPI-1) was used as a substrate in all experiments. It was cleaved in air, then loaded into the UHV system, and annealed at 700–900 K for several hours to remove contaminants. After the substrate cooled down to room temperature, high purity bismuth (99.999%) was evaporated from a ceramic crucible and deposited onto the

*pawel.kowalczyk@uni.lodz.pl
†simon.brown@canterbury.ac.nz

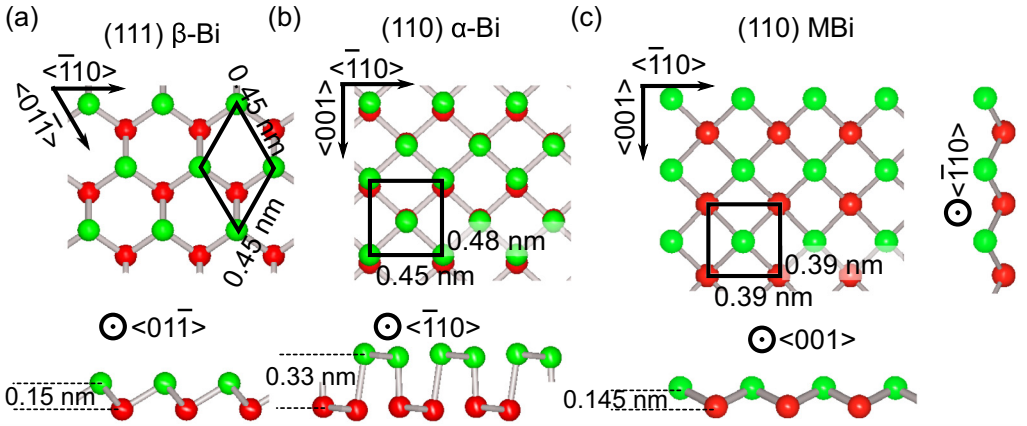

FIG. 1. Crystallographic structure of bismuth allotropes: (a) β-Bi [hexagonal, (111) structure], (b) α-Bi [(110) paired layer structure with rectangular unit cell], and (c) monolayer bismuth (MBi)—the new single layer rectangular structure reported here. Crystallographic directions, unit cells, and interlayer distances are marked in each case.

substrate at rates ~0.01 Å/s. The film thickness was monitored with a calibrated quartz crystal, and was measured in units of monolayers (ML). Here we define 1 ML as the thickness equivalent to that of a single rhombohedral Bi(110) plane, i.e., 3.3 Å [23].

STM measurements were carried out using an Omicron UHV STM at a base pressure of 10^{-8} Pa at 50 K (LT) and room temperature (300 K), using cut Pt90%-Ir10% tips. Typical scanning parameters used during measurements were $V_{\text{bias}} = -0.8$ V and $I = 10$ pA. STS measurements (± 1.0 V, 128 points per curve) were done in current imaging tunneling spectroscopy mode (CITS, 128×128 pts^2). All STS/CITS measurements were done at low temperature (LT). Measurement and data analysis procedures are similar to those described in Ref. [19]; dI/dV was calculated numerically and the presented data are spatial averages of ~100 dI/dV curves.

First-principles calculations of the electronic structure of freestanding MBi films were performed using Hartwigsen-Goedecker-Hutter-type (HGH) pseudopotentials and a plane-wave basis set, following methods discussed in detail previously [24,25]. The main program employed was developed by the ABINIT group. Spin-orbit coupling was included using the relativistic LDA approximation. Densities of states are calculated by integrating over the entire Brillouin zone. The vacuum layer thickness was 2 nm and the unit cell dimensions are discussed below.

III. RESULTS

The inset in Fig. 2(a) shows the typical morphology of the star-shaped Bi islands that grow on flat terraces of the HOPG substrate. Previous work [16–19,26–30] has shown that these islands have the α-Bi structure and a morphology which is characterized by large atomically flat island bases on top of which additional 2 ML high stripes are formed [26,28]. The stripes are parallel to the $\langle \bar{1}10 \rangle$ direction of the α-Bi lattice. In this work we focus on unusual single monolayer structures, identified here as MBi, which are occasionally found on the α-Bi bases. One MBi structure is highlighted by the the box in Fig. 2(a), and shown in greater detail in Fig. 2(b); other MBi structures can be observed to the left of the box in Fig. 2(a). The MBi structures have been observed many times, always between long parallel 2 ML α-Bi stripes. The lateral dimensions of the MBi are below 50 nm while their STM measured heights are 0.2 ± 0.1 nm (measured from the base). Experimental issues mean that it is difficult to measure the height more precisely but it is clearly different from the surrounding 2 ML stripes which are 0.66 ± 0.01 nm high [28]. In addition, a moiré pattern can be observed on top of the MBi,

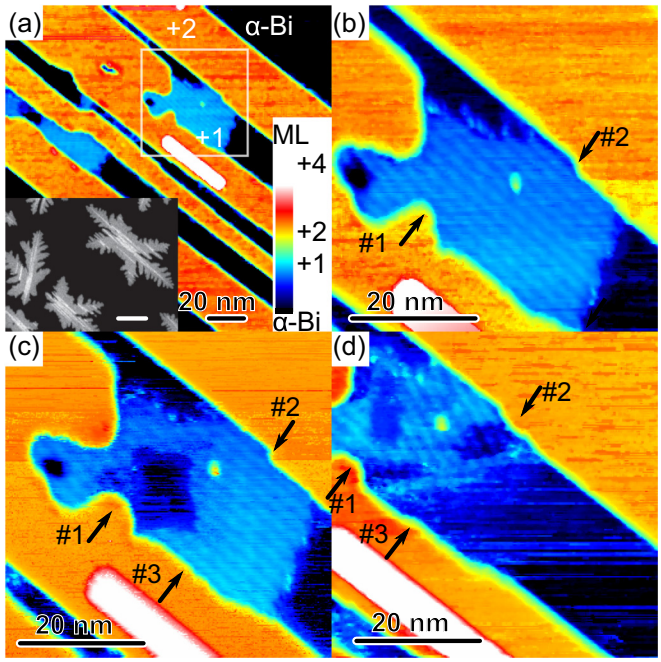

FIG. 2. (a) 150×150 nm^2 RT STM image showing magnification of large starlike shaped Bi island (inset: SEM image showing typical star-shaped islands, scale bar corresponds to 1 μm) with additional one monolayer thick MBi ad-layers (+1) grown on top of α-Bi base between stripes (+2). (b)–(d) Series of three 50×50 nm^2 STM images recorded in the region indicated by the square in (a), showing STM modification of the MBi ad-layer. Arrows marked #1–#3 show locations on the edges of the 2 ML stripes which changed during STM modification.

with a modulation that is almost (but not quite) parallel to the 2 ML stripes—this is discussed in detail below.

We find that MBi is always found in regions in which at least one of the neighboring stripes is defected [see Fig. 2(b), features labeled 1 and 2]. Extensive previous studies of the growth of bismuth islands and nanorods by diffusion and aggregation [18,19,23,26–30] suggest that the mechanism of MBi formation is that (i) Bi atoms land on the α-Bi surface during the deposition process, (ii) the atoms diffuse in the region between the long stripes, and (iii) these freely diffusing atoms are pinned by a defect (e.g., a kink in the stripe) which results in MBi nucleation.

In order to determine if the MBi is bonded to the underlying Bi atoms we used the STM tip to induce modification of the structure. First we zoom in to a selected region of the ad-layer (scan size 10×10 nm^2) using the usual setpoint current (10 pA), and then increase the setpoint current to 1 nA to reduce the tip-sample distance and increase the tip-sample interaction. After performing a full scan we reduce the setpoint current to 10 pA and enlarge the scan size in order to check if any morphological changes of the topography can be observed. The results of this series of experiments is shown in Figs. 2(b)–2(d). It is obvious that this procedure causes modification of the ad-layer—holes reaching the underlying α-Bi base are formed. Bi atoms initially located in the hole are often transferred to the stripes' edges which results in a morphology change. For example, in Figs. 2(b)–2(d) the protusion labeled #1 and the kink labeled #2 become rounded, and a new protrusion forms at #3. Note that when similar experiments are performed away from the ad-layer no changes to the bases and stripes are observed. These observations indicate that the observed ad-layer is weakly bonded to the supporting α-Bi base. It is an open question whether support by neighboring stripes is required to stabilize the MBi film, or whether the stripes merely allow nucleation of the MBi, as described above.

The crystallographic structure of the MBi can be deduced from atomic resolution images. Figures 3(a) and 3(b) clearly show a rectangularly arranged mesh of atoms which suggests strongly that we are dealing with a structure more similar to that of α-Bi [Bi(110)] then hexagonal β-Bi [Bi(111)]. The unit cell is estimated (from the atomic resolution images and fast Fourier transforms) to be $(0.40 \pm 0.02) \times (0.41 \pm 0.02)$ nm^2. These dimensions are much smaller than for bulk Bi(110) (0.455×0.475 nm^2) [31] and Bi(110) films on HOPG ($0.45 \pm 0.02 \times 0.48 \pm 0.02$ nm^2) [18,28–30], indicating an $\sim$10% compression of the MBi unit cell with respect to the underlying α-Bi base.

This difference in unit cells of the MBi and α-Bi manifests itself also by formation of a moiré pattern observed by STM as in Figs. 2(a)–2(d) and 3(a) and 3(b), i.e., there is a periodic modulation of the apparent height in a direction nearly parallel to the 2 ML stripes (this is the Bi$\langle\bar{1}10\rangle$ direction [26]). This additional modulation is more clearly visible in some images than others, e.g., it is less clear in Fig. 3(b) than in Fig. 3(a). The moiré pattern periodicity is estimated to be $\sim$2.0 nm and its orientation differs by $\sim 6^\circ$ with respect to the atomic rows, i.e., to the $\langle\bar{1}10\rangle$ direction [see blue and red lines in Fig. 3(b)]. Close inspection of Fig. 3(a) reveals that the intensity along each moiré stripe is additionally modulated with periodicity of $\sim$3 nm. The angle between these two periodicities is estimated to $80^\circ \pm 10^\circ$. A further important feature of the data is that after modification the moiré pattern rotates by $\sim 20^\circ$ but does not change its period significantly.

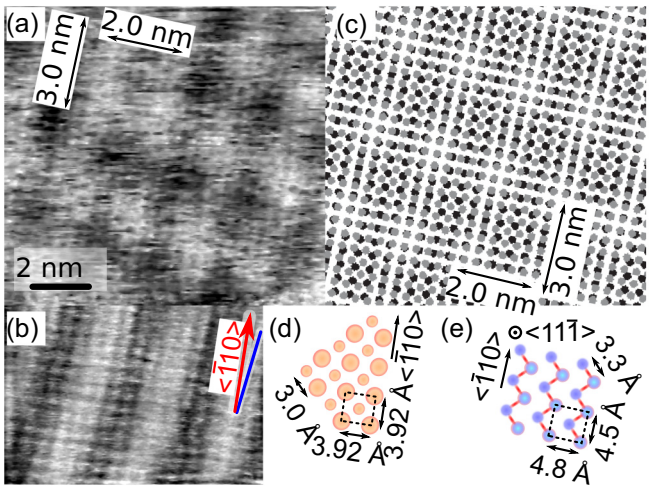

FIG. 3. (a) LT STM image (−0.8 V, 0.2 nA) showing clear moiré pattern recorded on MBi. (b) Further high resolution STM image with clear atomic resolution; red and blue bars indicate the direction of overlayer atoms and moiré pattern, respectively. (c) Moiré pattern simulation obtained by superposition of the two unit cells shown in (d) and (e). Only the corner atoms in each unit cell are shown because the puckering effect (see side views, Fig. 1) means that the other atom in the unit cell is in a different plane and not usually visible in the STM measurements. Periodicities of both moiré patterns are indicated in (a) and (c).

We explain the experimental observations using a simple superposition model [30]. Figure 3(c) shows the result of superposing MBi with unit cell 0.392×0.392 nm^2 on α-Bi with unit cell 0.450×0.480 nm^2 [see Figs. 3(d) and 3(e) for ball models for the individual layers]. This combination nicely reproduces the experimentally observed features: the moiré periodicities are $\sim$2.0 and $\sim$3.0 nm as in Fig. 3(a), the angle between them is 78°, and the angle between the atomic rows and the moiré pattern is 4°. Additionally, on rotation of the MBi layer by 4° with respect to the α-Bi layer we find that the period of the moiré pattern is unchanged even though its angle with respect to the Bi$\langle\bar{1}10\rangle$ direction changes by $\sim 20^\circ$, as is observed experimentally [Figs. 2(c) and 2(d)]. This (lack of) angular dependence, along with an exquisite sensitivity of the moiré periodicity to changes in the MBi unit cell, allows a much more precise determination of the MBi lattice parameter than the atomic resolution images in Fig. 2, i.e., 0.39 nm, with an uncertainty smaller than 0.01 nm [32].

In Fig. 4(a) we show results of our STS experiments. dI/dV curves #1 and #2 were recorded on the α-Bi base and MBi, respectively. In the ± 1 eV range the local density of states for the α-Bi is characterized by two distinct peaks located at ~ -0.3 and $\sim +0.5$ eV [19]. The dI/dV curve for the MBi (#2) is characterized by the presence of three maxima located at -0.1, $+0.1$, and $+0.4$ eV.

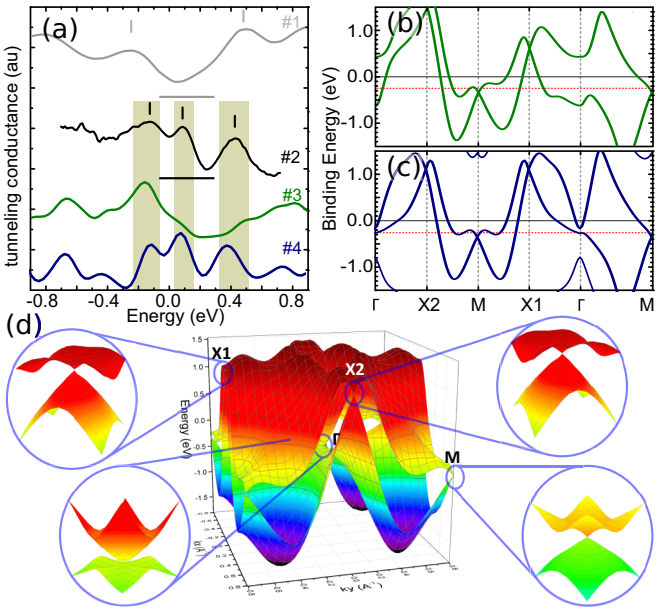

FIG. 4. (a) Tunneling conductance spectra recorded for α-Bi (#1), MBi (#2), together with the DOS calculated using DFT for 0.37×0.41 nm^2 (#3) and 0.39×0.39 nm^2 (#4) unit cells. Shaded rectangles highlight the positions of the three main experimental peaks for MBi. (b) Band diagram for 3.7×4.1 nm^2 and (c) 0.39×0.39 nm^2 unit cells. (d) 3D plot of the band structure shown in (c). The red dotted lines in (b) and (c) indicate the location of the Fermi levels used to shift #3 and #4 in (a) (0.25 and 0.28 eV, respectively).

IV. DFT CALCULATIONS AND DISCUSSION

To understand the electronic structure of the MBi we have performed DFT calculations to determine the minimum energy structures and also to investigate the band structure. A $17 \times 17 \times 1$ sampling grid in momentum space was employed in accordance with the Monkhorst-Pack method and the cutoff of electron kinetic energy was set to 400 eV. The atomic positions were allowed to relax from the default bulk values by energy minimization until the Hellmann-Feynman forces were reduced to below 1.0×10^5 eV/Å. We find that a single monolayer of α-Bi is not stable—this is expected, because the second layer in the paired layer structure is required to hold it together. Remarkably, however, we find that a single monolayer structure with symmetry similar to that of the Bi(110) structure is stable if it is considerably contracted with respect to that of the Bi(110) structure.

We find that the minimum energy structure obtained after full optimization has a unit cell with dimensions 0.37×0.41 nm^2 [the band structure is shown in Fig. 4(b)]. We also consider a structure that is constrained to have a square unit cell with the dimensions 0.39×0.39 nm^2 that best match the atomic resolution and moiré measurements discussed above [band structure shown in Fig. 4(c)]. Then our DFT calculations show that the energy is minimized when the middle atom is located at $(0.47a, 0.50a)$ where $a = 0.39$ nm and is displaced vertically by 0.145 nm [see Fig. 1(c)]. The energy of this structure is only slightly higher (-306.55 versus -306.58 eV/unit cell) than for the 0.37×0.41 nm^2 structure but is significantly lower than for the unstable single monolayer of α-Bi (-306.11 eV/unit cell). These freestanding monolayer structures all have higher energy than 2 ML α-Bi ($\frac{1}{2} \times -613.70$ eV/unit cell $= -306.85$ eV/unit cell/ML), but we expect that the interaction with the underlying substrate most probably changes the energy balance and makes the MBi structures more stable. Unfortunately, it is computationally too expensive to simulate the whole incommensurate structure, because it requires a very large supercell.

Figure 4(a) shows that the calculated DOS for the 0.39×0.39 nm^2 structure (curve #4) is in excellent agreement with the experimental STS data (curve #2). The shading highlights the good agreement in the number of the main peaks in the spectrum, and their positions after taking into account small shifts in the Fermi level due to doping from the substrate [33] (the precise doping mechanism is unclear and requires further investigation). In contrast, the calculated DOS for the 0.37×0.41 nm^2 unit cell (#3) does not reproduce all the features of the experimental data. Taking into consideration the unit cell measured using STM, the good fit of moiré simulations to the experimentally observed data, and the good agreement with calculated density of states it is clear that the MBi films grow in the 0.39×0.39 nm^2 structure instead of minimum energy one.

The two bands evident in Figs. 4(b) and 4(c) originate from the unsaturated Bi-6p orbitals of the two atoms in the unit cell. Of particular interest is the existence of two-dimensional Dirac cones in the band structure of MBi films (which are in some ways similar to those observed in topological metals [34,35]). As shown in Figs. 4(b) and 4(c), for both the 0.39×0.39 and 0.37×0.41 nm^2 structures, the two bands cross each other at the M, $X1$, and $X2$ points, and because the bands have opposite parity eigenvalues they form three two-dimensional Dirac cones. The Dirac points at M and $X2$ are protected by the mirror reflection symmetry of the lattice. However a small energy gap (not visible on this scale) is opened at the Dirac point at $X1$ because the mirror symmetry is broken by the displacement of the central atom within the unit cell [Fig. 1(c)]. Reference [25] discusses these symmetry issues for Bi films with odd-layer thicknesses in more detail and shows that—in contrast with graphene—the strong spin-orbit coupling in MBi is essential for creating Dirac cones in this system. Therefore, the MBi films realized here are a unique opportunity for investigating strongly spin-orbit coupled 2D Dirac fermions.

V. CONCLUSIONS

The MBi structure reported here is a new allotrope which was neither observed nor predicted previously, and is the first monolayer bismuth structure observed with rectangular symmetry. In its present form the MBi is only observed relatively rarely and appears to rely on nucleation at defects and imperfections in supporting Bi(110) stripe structures, but similar structures might be realized among other materials in the 15$^{\text{th}}$ group of the periodic table and/or by careful choice of alternate substrates. Clearly further work is required to determine whether larger areas of the novel monolayer structure can be obtained by this or other synthesis methods, and microelectronics compatible substrates are required to allow transport measurements that exploit the multiple Dirac cones that are the key features of the band structure.

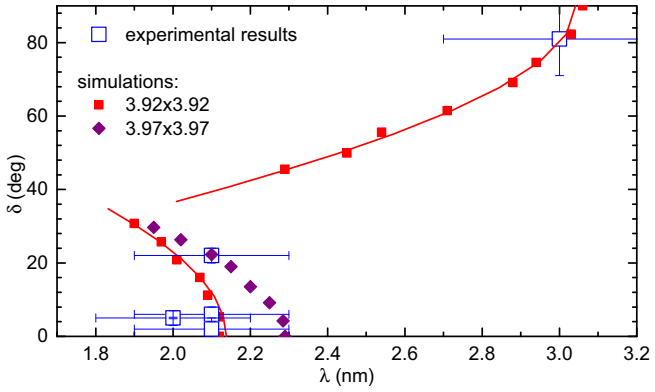

FIG. 5. Angle between moiré pattern and substrate direction δ versus moiré periodicity λ for experimental data (open squares) and two simulated square unit cells 3.92×3.92 nm^2 (filled squares) and 3.97×3.97 nm^2 (filled diamonds). Each data point corresponds to a different angle of rotation between the MBi overlayer and the underlying α-Bi.

ACKNOWLEDGMENTS

This work was supported by the Polish National Science Centre (DEC-2015/17/B/ST3/02362, P.J.K.), the Marsden Fund and MacDiarmid Institute for Advanced Materials and Nanotechnology (O.M. and S.A.B.), the National Natural Science Foundation of China (11204133, X.W.), and the U.S. National Science Foundation (NSF-DMR-1305583, T.-C.C.).

APPENDIX: MOIRÉ PATTERN SIMULATION

Our moiré simulations are presented in Fig. 5, which compares the modeled period and rotation angle of the moiré pattern with the experimental values. We have performed a series of simulations and explored a range of unit cells for the overlayer (including models both with and without the central atom in the unit cell). We find that an MBi unit cell of 3.92×3.92 Å^2 with no central atom uniquely explains (red symbols) the values of the moiré periodicity and lack of angular dependence of the moiré pattern. Note that it also explains the second moiré periodicity (in the orthogonal direction, experimental data point at the top right of Fig. 5). To demonstrate the exquisite sensitivity of the moiré pattern periodicity to changes in the MBi unit cell we also show (purple diamonds) the variation of periodicity with rotation angle for an MBi unit cell of 3.97×3.97 Å^2. The purple diamonds do not agree well with the experimental data—evidently the uncertainty in the MBi unit cell dimensions is smaller than 0.1 Å.

[1] K. S. Novoselov, A. K. Geim, S. V. Morozov, D. Jiang, M. I. Katsnelson, I. V. Grigorieva, S. V. Dubonos, and A. A. Firsov, Nature (London) **438**, 197 (2005).
[2] A. H. Castro Neto, F. Guinea, N. M. R. Peres, K. S. Novoselov, and A. K. Geim, Rev. Mod. Phys. **81**, 109 (2009).
[3] A. C. Ferrari, F. Bonaccorso, V. Fal'ko, K. S. Novoselov *et al.*, Nanoscale **7**, 4598 (2015).
[4] A. J. Mannix, B. Kiraly, M. C. Hersam, and N. P. Guisinger, Nat. Rev. Chem. **1**, 0014 (2017).
[5] A. Kara, H. Enriquez, A. P. Seitsonen, L. L. Y. Voon, S. Vizzini, B. Aufray, and H. Oughaddou, Surf. Sci. Rep. **67**, 1 (2012).
[6] M. E. Dávila, L. Xian, S. Cahangirov, A. Rubio, and G. L. Lay, New J. Phys. **16**, 095002 (2014).
[7] E. Bianco, S. Butler, S. Jiang, O. D. Restrepo, W. Windl, and J. E. Goldberger, ACS Nano **7**, 4414 (2013).
[8] K. S. Novoselov, D. Jiang, F. Schedin, T. J. Booth, V. V. Khotkevich, S. V. Morozov, and A. K. Geim, Proc. Natl. Acad. Sci. USA **102**, 10451 (2005).
[9] B. Radisavljevic, A. Radenovic, J. Brivio, V. Giacometti, and A. Kis, Nat. Nanotechnol. **6**, 147 (2011).
[10] H. S. S. Ramakrishna Matte, A. Gomathi, A. K. Manna, D. J. Late, R. Datta, S. K. Pati, and C. Rao, Angew. Chem. **122**, 4153 (2010).
[11] Z. Zeng, Z. Yin, X. Huang, H. Li, Q. He, G. Lu, F. Boey, and H. Zhang, Angew. Chem. Int. Ed. **50**, 11093 (2011).
[12] L. Li, Y. Yu, G. J. Ye, Q. Ge, X. Ou, H. Wu, D. Feng, X. H. Chen, and Y. Zhang, Nat. Nanotechnol. **9**, 372 (2014).
[13] J. Wood, S. Wells, D. Jariwala, K.-S. Chen, E. Cho, V. Sangwan, X. Liu, L. J. Lauhon, T. Marks, and M. Hersam, Nano Lett. **14**, 6964 (2014).
[14] O. Osters, T. Nilges, F. Bachhuber, F. Pielnhofer, R. Weihrich, M. Schöneich, and P. Schmidt, Angew. Chem., Int. Ed. **51**, 2994 (2012).
[15] Z. F. Wang, L. Chen, and F. Liu, Nano Lett. **14**, 2879 (2014).
[16] S. Zhang, M. Xie, F. Li, Z. Yan, Y. Li, E. Kan, W. Liu, Z. Chen, and H. Zeng, Angew. Chem., Int. Ed. **55**, 1666 (2016).
[17] T. Nagao, J. T. Sadowski, M. Saito, S. Yaginuma, Y. Fujikawa, T. Kogure, T. Ohno, Y. Hasegawa, S. Hasegawa, and T. Sakurai, Phys. Rev. Lett. **93**, 105501 (2004).
[18] P. J. Kowalczyk, D. Belic, O. Mahapatra, S. A. Brown, E. S. Kadantsev, T. K. Woo, B. Ingham, and W. Kozlowski, Appl. Phys. Lett. **100**, 151904 (2012).
[19] P. J. Kowalczyk, O. Mahapatra, S. A. Brown, G. Bian, X. Wang, and T.-C. Chiang, Nano Lett. **13**, 43 (2013).
[20] G. Wang, R. Pandey, and S. P. Karna, ACS Appl. Mater. Interfaces **7**, 11490 (2015).
[21] M. Wada, S. Murakami, F. Freimuth, and G. Bihlmayer, Phys. Rev. B **83**, 121310 (2011).
[22] Y. Lu, W. Xu, M. Zeng, G. Yao, L. Shen *et al.*, Nano Lett. **15**, 80 (2015).
[23] S. A. Scott, M. V. Kral, and S. A. Brown, Phys. Rev. B **72**, 205423 (2005).
[24] G. Bian, T. Miller, and T.-C. Chiang, Phys. Rev. B **80**, 245407 (2009).
[25] G. Bian, X. Wang, T. Miller, T.-C. Chiang, P. J. Kowalczyk, O. Mahapatra, and S. A. Brown, Phys. Rev. B **90**, 195409 (2014).
[26] S. A. Scott, M. V. Kral, and S. A. Brown, Phys. Rev. B **73**, 205424 (2006).
[27] D. N. McCarthy, D. Robertson, P. J. Kowalczyk, and S. A. Brown, Surf. Sci. **604**, 1273 (2010).

[28] P. J. Kowalczyk, O. Mahapatra, D. N. McCarthy, W. Kozlowski, Z. Klusek, and S. A. Brown, Surf. Sci. **605**, 659 (2011).
[29] P. J. Kowalczyk, D. Belić, O. Mahapatra, and S. A. Brown, Acta Mater. **60**, 674 (2012).
[30] P. J. Kowalczyk, O. Mahapatra, D. Belić, S. A. Brown, G. Bian, and T.-C. Chiang, Phys. Rev. B **91**, 045434 (2015).
[31] P. Hofmann, Prog. Surf. Sci. **81**, 191 (2006).
[32] D. A. Cosma, J. R. Wallbank, V. Cheianov, and V. I. Fal'ko, Faraday Discuss. **173**, 137 (2014).
[33] I. Gierz, C. Riedl, U. Starke, C. R. Ast, and K. Kern, Nano Lett. **8**, 4603 (2008).
[34] H. Ji, I. Pletikosić, Q. D. Gibson, G. Sahasrabudhe, T. Valla, and R. J. Cava, Phys. Rev. B **93**, 045315 (2016).
[35] J. Nayak, S.-C. Wu, N. Kumar, C. Shekhar, S. Singh, J. Fink, E. E. D. Rienks, G. H. Fecher, S. S. P. Parkin, B. Yan, and C. Felser, Nat. Commun. **8**, 13942 (2017).